

Spin memory of the topological material under strong disorder

Inna Korzhovska,¹ Haiming Deng,¹ Lukas Zhao,¹ Zhiyi Chen,¹ Marcin Konczykowski,² Shihua Zhao,¹ Simone Raoux,³ & Lia Krusin-Elbaum^{1,†}

¹*Department of Physics, The City College of New York - CUNY, New York, NY 10031, USA*

²*Laboratoire des Solides Irradiés, École Polytechnique, CNRS,*

CEA, Université Paris-Saclay, 91128 Palaiseau cedex, France and

³*Helmholtz-Zentrum Berlin für Materialien und Energie, 12489 Berlin, Germany*

(Dated: August 24, 2021)

Robustness to disorder – the defining property of any topological state – has been mostly tested in low-disorder translationally-invariant materials systems where the protecting underlying symmetry, such as time reversal, is preserved. The ultimate disorder limits to topological protection are still unknown, however a number of theories predict that even in the amorphous state a quantized conductance might yet reemerge. Here we report a directly detected robust spin response in structurally disordered thin films of the topological material Sb_2Te_3 *free of extrinsic magnetic dopants*, which we controllably tune from a strong (amorphous) to a weak (crystalline) disorder state. The magnetic signal onsets at a surprisingly high temperature (~ 200 K) and eventually ceases within the crystalline state. We demonstrate that in a strongly disordered state *disorder-induced spin correlations* dominate the transport of charge — they engender a spin memory phenomenon, generated by the nonequilibrium charge currents controlled by localized spins. The negative magnetoresistance (MR) in the extensive spin-memory phase space is isotropic. Within the crystalline state, it transitions into a positive MR corresponding to the weak antilocalization (WAL) quantum interference effect, with a 2D scaling characteristic of the topological state. Our findings demonstrate that these nonequilibrium currents set a disorder threshold to the topological state; they lay out a path to tunable spin-dependent charge transport and point to new possibilities of spin control by disorder engineering of topological materials

Electronic disorder [1] and elementary excitations in quantum condensed matter are fundamentally linked and it is well established that spatially fluctuating potentials tend to promote decoherence and localization of fermions, i.e. formation of Anderson insulators [2]. The interplay of interactions and disorder often leads to new quantum behaviors; disorder typically boosts interparticle correlations both in charge and in spin channels, and that could either aid or suppress the motion of charge [3]. Spin effects related to disorder are particularly important when spin-orbit coupling (SOC) is strong [4], and when spin-dependent charge transport can be electrically manipulated for uses, e.g. in spin-based electronics [5].

Strong SOC is a hallmark of three-dimensional (3D) topological insulators [6], where 2D gapless spin-polarized Dirac surface states are robust against backscattering. Most topological materials are known to contain a natural population of charged defects [7] that do not cause a destruction of the topological Dirac states [8]; indeed, they can be compensated [9] as long as Dirac mass [10] or puddle [11] disorders do not enter. Under weak disorder, a coherent interference of electron waves survives disorder averaging [12], and strong SOC enhances conductivity by a weak antilocalization (WAL) correction related to the topological π -Berry phase [6] when magnetic impurities are absent. The 2D WAL channels can be outnumbered by the weak localization (WL) channels [13] — this is a precursor of Anderson localization [2], which occurs at strong disorder. Under strong disorder, theory and numerical simulations [14–17]

predict an emergence of a new topological state, dubbed ‘topological Anderson insulator’, in which conductance $G_0 = 2e^2/h$ is quantized. Indeed, recent theoretical demonstrations of topological phases in amorphous systems [18, 19] point to promising new possibilities in engineered random landscapes. Strong disorder, however, is not trivial to install, quantify and control, and topological matter under such conditions has not yet been experimentally tested.

Here we implement an extensive range of site disorder – from amorphous to crystalline state – in Sb_2Te_3 , the material which is a known 2nd generation topological insulator [20–22], and report that under strong structural and electronic disorder conditions dynamic spin correlations dominate charge transport over a surprisingly large range of magnetic fields. These correlations imprint spin memory on the electrons hopping via localized spin sites. Predicted to be small [23] and thus practically unobservable in the conventional materials, the effect found here is large; it persists over a surprisingly wide range of disorder and well within the disordered crystalline topological phase, as long as variable range electron hopping (VRH) [24] is at play. It eventually transitions into the characteristic 2D WAL regime when the gapless surface channels are reestablished. The spin memory uncovered in this work is *not an orbital effect*; it is distinct from the weak localization interference effect (WL) observed in the magnetically doped topological insulators [25]. It originates from the presence of disorder-induced localized spins [3] and, as witnessed by the characteristically non-analytic

negative magnetoresistance (neg-MR), is governed by the distribution of very large spin g -factors that widens with decreasing localization length ξ in a way akin to an assembly of quantum wells [26].

The experiments were performed on thin ($\sim 20 - 50$ nm) films of Sb_2Te_3 , in which extreme positional disorder (amorphous state) is possible to obtain (SI, Section A). Sb_2Te_3 is a well known phase-change material [27] (SI, Fig. S1), that undergoes amorphous-to-crystalline transformation with the concurrent orders-of-magnitude resistive drop, and hence a huge range of disorder could be controllably explored.

Let us recall that in the presence of disorder a finite population of singly occupied states below the Fermi energy E_F has been discussed as long as 20 years back by Sir Neville Mott [3]. Magnetic response from randomly localized spins in such state was expected to be weak and, as far as we know, has never been experimentally demonstrated. So our first surprising finding was a very robust magnetic signal from the disordered Sb_2Te_3 films directly detected using a custom-designed μ Hall sensors (Figs. 1A,B), with the thin film flakes mechanically exfoliated from their substrates and transferred onto the active sensor area (Materials and Methods, SI, Fig. S2). Our films do obey Anderson scaling (see Fig. 1C), and we surmise that here the observed effective moment per atom is significantly amplified by the large effective Landé g -factor [4] in Sb_2Te_3 , where SOC is strong [20]. The detected signal depends on the magnetic history (field-cooling *vs.* zero-field cooling), which, together with slow magnetic relaxation (Fig. S2C) reflects a glassy nature of the localized state. We emphasize that magnetic signal crucially depends on the level of disorder; indeed, it becomes barely detectable in the crystalline phase as disorder in *the same film* is reduced by thermal annealing (Fig. 1B).

Our second key finding is shown in Fig. 1D. The change in the longitudinal magnetoresistance ΔR_{xx} at low magnetic fields is with a remarkable fidelity impervious to the tilt of magnetic field. It is relatively large and negative (i.e. charge transport becomes less dissipative) up to a field H_{max} (Figs. 1D and S3). This field isotropy of the low-field dissipation ‘quench’ naturally suggests a spin-dominated mechanism rather than orbital effect, and so the pertinent question to ask is how such behavior can proceed in a system where electronic states are localized and the *extrinsic* spinfull impurities are absent (Table S1).

With strong disorder charge transport is a complex electron hopping process that at low temperatures proceeds via quantum tunneling between localized states assisted by phonons [24, 30]. While considerations of magnetotransport have mainly focused on the orbital effects, a recently proposed idea [23] takes note of putative nonequilibrium spin correlations in the localized regime created by the flowing current when electron hopping

times τ are short relative to the spin relaxation times τ_s . These time scales determine the magnetic field range over which spin-correlation-driven neg-MR (positive magnetoconductance) ought to be present. The idea is illustrated in Fig. 1E. When the current is injected, an electron with spin \mathbf{S} attempting to hop to an available empty site can do it in two ways: directly or via an intermediate site occupied by a localized spin \mathbf{s} . It may take several attempts for the indirect hops to succeed and the return probability will depend on history, i.e. on whether the tunneling electron can form a triplet or a singlet state with \mathbf{s} . For example, in the absence of disorder a triplet state would remain so in the presence of applied magnetic field and no reduction of magnetoresistance (increase of magnetoconductance) is expected. Under strong disorder (such as shown in Fig. 1C), however, spin g -factors will be spatially random so that localized spins at different sites will precess incoherently and spin correlations will be destroyed by the field. Accordingly, in a simple model [23] the change in magnetoconductance ΔG_{xx} arising from such spin correlations should follow not a power law [31] but a unique non-analytic form:

$$\frac{\Delta G_{xx}(H)}{G_{xx}(0)} \sim A \left[-\Gamma \left(-\frac{d_s}{2} \right) \right] \sum_{l=-1}^1 \left[\left(\frac{ilH}{H^{**}} + \frac{\tau}{\tau_s} \right)^{d_s/2} - \left(\frac{\tau}{\tau_s} \right)^{d_s/2} \right], \quad (1)$$

where $A = \frac{G_{xx}(H \rightarrow \infty) - G_{xx}(0)}{G_{xx}(0)}$, $d_s = 4/3$ is the spectral dimension of the percolation cluster [32] (which is the relevant dimension in the hopping process), l is index of the diffusing spin, $\Gamma(-\frac{d_s}{2})$ is the gamma function $\cong -4$, and $H^{**} = \frac{\hbar}{\mu_B \tau \Delta g}$ is the limiting magnetic field range set by the hopping rate $1/\tau$ and the disorder-induced spread Δg of spin g -factors.

The strongly localizing behavior we observe in the longitudinal resistance R_{xx} (Fig. 2A) at low temperatures (below ~ 10 K) follows variable range hopping law $R_{xx}(T) = R_0 \exp(\frac{T_0}{T})^{1/2}$ of Efros-Shklovskii (E-S) kind [30], see Fig. 2B. The E-S energy scale T_0 characteristic of the hopping process (Fig. S1B) is tracked on decreasing disorder by a well controlled thermal annealing schedule (Materials and Methods); it is inversely proportional to the electron localization length [24] ξ , which we will show controls the g -factor distribution width Δg . We remark that in this regime (at low T) the detected magnetic moment appears ‘flat’ in temperature (Fig. 1B).

In the variable range hopping (VRH) regime, the fit of conductance to Eq. (1) for two states of disorder is illustrated in Fig. 2C. As seen in the figure, at low magnetic fields the characteristic non-analytic behavior is accurately followed; here the ratio of hopping time to spin relaxation time τ/τ_s and the hopping field scale H^{**} were

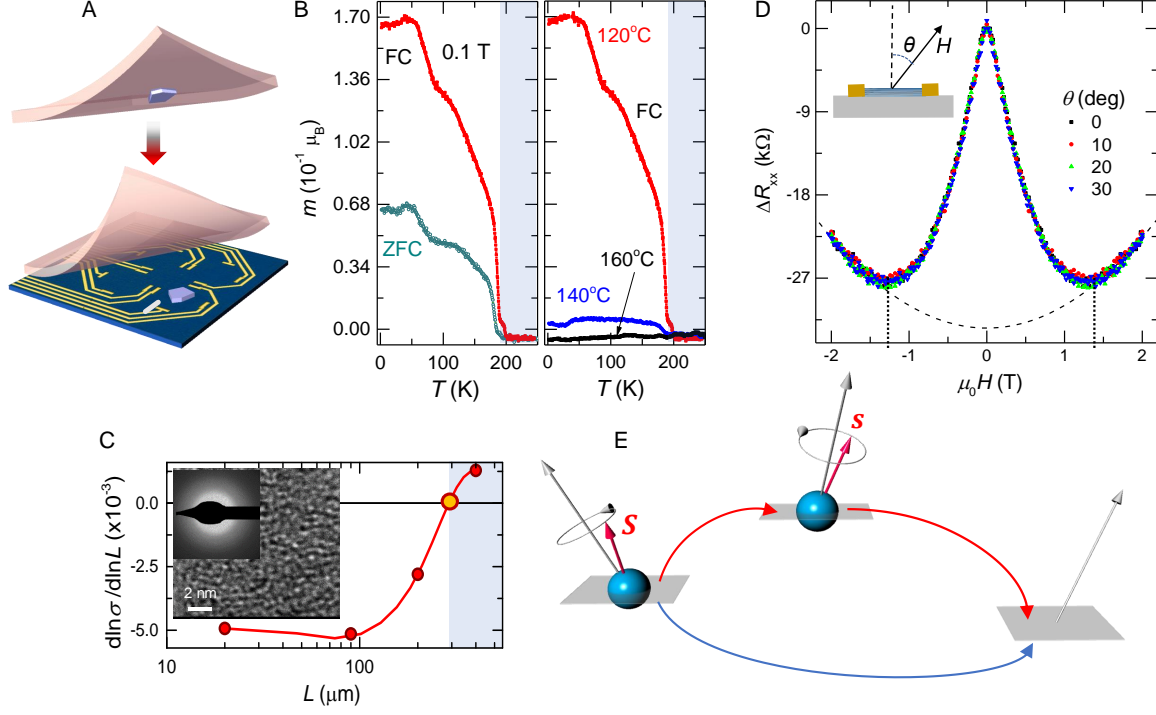


FIG. 1. Non-equilibrium spin correlations in strongly disordered Sb_2Te_3 . (A), Thin (20 nm) Sb_2Te_3 flakes were exfoliated and transferred atop a μ -Hall sensor (Methods). The scale bar is 50 μm . (B), Magnetic moment per atom, m , measured by a μ -Hall sensor. *Left*: m in a 0.1 T field under field-cooling (FC) and zero-field-cooling (ZFC) conditions. *Right*: m of the same flake for three levels of disorder indexed by annealing temperature T_a . It onsets at ~ 200 K, saturates at low T , and becomes vanishingly small for $T_a \gtrsim 160^\circ\text{C}$. (C), As-deposited Sb_2Te_3 films are amorphous as seen by the transmission electron microscopy (inset). The lateral size L dependence of longitudinal conductivity σ obeys Anderson scaling [1]. (D), Longitudinal resistance $R_{xx}(H)$ of strongly disordered Sb_2Te_3 films ($T_a = 120^\circ\text{C}$) does not depend on the tilt of magnetic field (see sketch). The dissipation reduction is relatively large (several %); it is observed below H_{max} , the field at which $\Delta R_{xx}(H)$ crosses over to the H^2 -dependence (dash). Data in (C) and (D) were taken at 1.9 K. (E), Cartoon of electron hopping to a distant empty site under flowing current, see text. The electron with spin S may reach this site directly or via an intermediate site hosting localized spin s . Random disorder landscape induces spatial randomness in the spin g -factors and hence the randomness of local fields (grey arrows) controlling the precession of all spins. The indirect channel will depend on the state of s during hopping attempts and the memory of this state is encoded in the transport of charge. These spin correlations are destroyed by magnetic field, and consequently the resistance is reduced.

used as fitting parameters (Materials and Methods). The fits at different disorder levels controlled by the anneals at different temperatures T_a are shown in Fig. S4. The ratio τ/τ_s strongly depends on the level of disorder (Fig. 2D), with the hopping and spin relaxation rates, $1/\tau \propto H^{**}$ and $1/\tau_s \propto H_s$, in close correspondence with the disorder dependence of R_{xx} all the way through crystallization transition (see Fig. 5 below). The hopping time τ can be independently extracted from the E-S energy (Fig. S5A), and, as expected for the hopping conductivity τ increases exponentially on decreasing temperature (Fig. S5B). This allows us to consistently obtain the evolution of spin-relaxation time τ_s (Fig. 2E) and Δg (Fig. 3A) with decreasing disorder (increasing T_a), and hence that of the low-field spin-relaxation scale $H_s = \frac{\hbar}{\mu_B \tau_s \Delta g}$ (Fig. S6); H_s marks a crossover from the concave-up field shape associated with τ_s to concave-down behavior at higher fields,

see Fig. 2C.

An intriguing question arises as to what controls the unexpectedly large (Tesla-range) field scale where negative magnetoresistance, the hallmark of dynamic spin memory, is found. For the material systems with small spin-orbit coupling where g -factor ~ 2 , the expected field range would be in the $10^{-4} - 10^{-5}$ Tesla range. In theory [23], this field scale is obtained from the competition of the magnetic energy of the spins, $g\mu_B H$, and either thermal energy or the exchange energy J between neighboring spins – it ought to be well below the competing effects. Here, however, with large effective g value [33], $g\mu_B H/k_B \sim 20$ K is comparable to the spin-memory range. This brings us back to disorder-induced spin correlations. Fig. 1B shows that under extreme disorder the onset of magnetic response is abrupt and at a remarkably high temperature $T_s \sim 200$ K. While the details

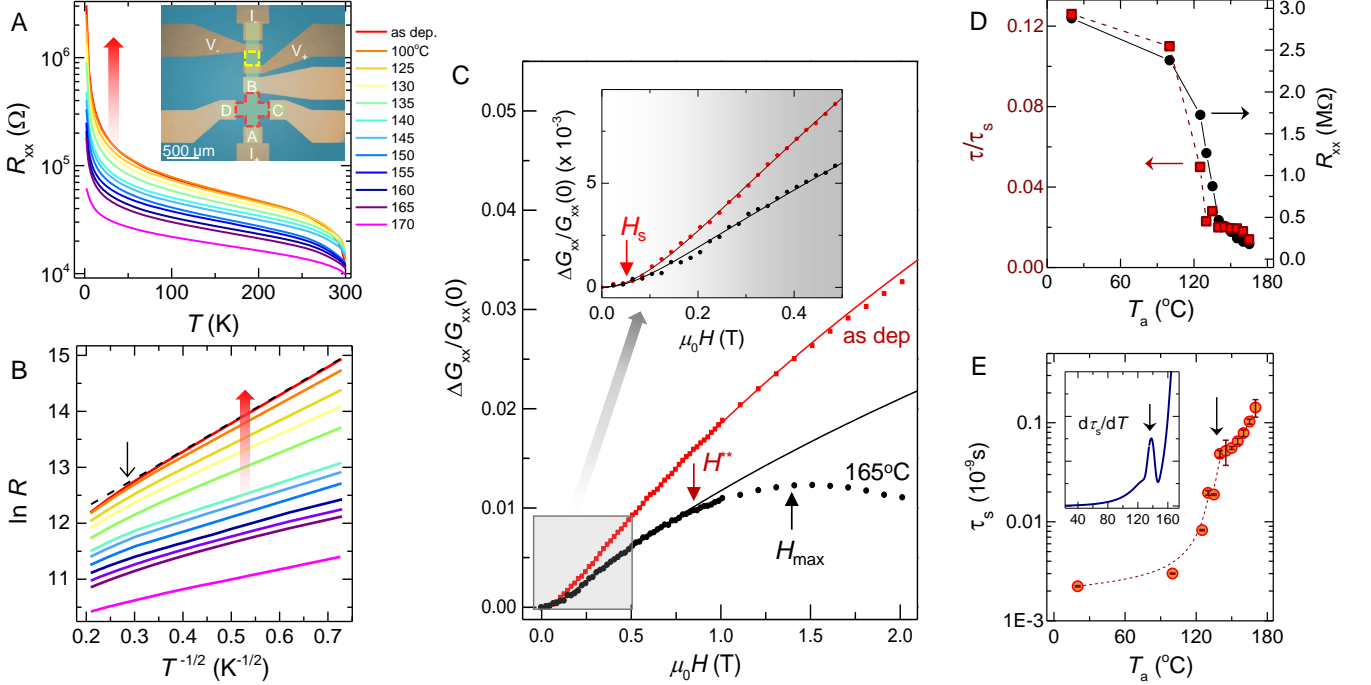


FIG. 2. Spin memory effect in the longitudinal conductance G_{xx} of Sb_2Te_3 in the VRH regime. (A), $R_{xx}(T)$ of a 20 nm thin Sb_2Te_3 film under strong disorder increases at low temperatures by orders of magnitude; the strength of disorder is reproducibly controlled by T_a . Inset: lithographically patterned Hall-bar and van der Pauw contact configurations used in measurements of R_{xx} . (B), R_{xx} exponential in inverse \sqrt{T} confirms that below ~ 10 K charge transport is by the 3D VRH [24], the regime where dynamic spin correlation are expected. The color code is as in (A)). Red arrows in ((A) and (B)) point in the direction of increasing disorder. (C), Field dependence of G_{xx} for two disorder states shown at 1.9 K. A fit (solid lines) to Eq. (1) fully reproduces the non-analytic form of $\Delta G_{xx}(H)/G_{xx}(0)$ arising from spin-memory in the VRH regime. Inset: Zoom of the data at low fields. (D), Disorder dependence of τ/τ_s , the ratio of hopping to spin-relaxation time, is found to closely correlate with the low- T R_{xx} . (E), τ_s increases by nearly two orders of magnitude in the disorder range studied; it is a very sensitive probe of the phase change at crystallization, see inset.

of spin correlations in this Anderson-like-localized glassy state clearly deserve further experimental and theoretical studies, a rough estimate of $J \sim k_B T_s / z \approx 70$ K, using local coordination number [27] $z \sim 3$ expected in Sb_2Te_3 , implies that here short range interactions between localized spins play the key role (see SI, Section A).

Let us now consider g -factor fluctuations in a strongly disordered state. The g distribution width naturally arising from our magnetoconductance data (Fig. 3A) within the model considered above is spectacularly wide at the highest level of disorder, $\Delta g \simeq 40$; indeed, it exceeds the effective g value of ~ 30 obtained *e.g.* directly in the same topological insulator family from the electron spin resonance (ESR) experiments [33]. Such large g spread is uncommon but not unprecedented. Giant fluctuations of g -factors have been reported in *e.g.* InAs nanowires where $\Delta g > |g_{eff}|$ and the effective factor $|g_{eff}|$ is also large [29]. Furthermore, in semiconducting quantum wells $|g_{eff}|$ has been known to increase roughly linearly [26] with quantum confinement energy

E_Q as $|g_{eff}| \simeq g_0 + \beta E_Q$, where β is a material-specific constant. Here we propose that in the strongly localized Anderson-like state, quantum confinement is enforced by the wells constrained by the localization length ξ (Fig. 3B). In this view, a simple particle-in-a-box approximation gives $E_Q \propto \xi^{-2}$ that indeed fully scales with Δg (Fig. 3A). The expected linear $|g_{eff}|$ vs. E_Q would then set $|g_{eff}| \sim \Delta g^{-\alpha}$ with $\alpha \sim 0.1$, with $|g_{eff}|$ approaching the ESR-determined value in the unconfined state, see Fig. 3C.

Our experiments reveal that positive $\Delta G_{xx}(H)$ (neg-MR), evolves progressively with decreasing disorder; it persists over a spectacularly large disorder range, all the way through the crystallization process and beyond (Fig. 4A). The large limiting field range set by H_{max} at strong disorder falls with increasing T_a (Fig. 4B) to pinch off $\Delta G_{xx}(H)$ eventually to null. A clear visual of the field-disorder phase space is shown in Fig. 4C, where the strength of disorder is represented by E_Q . $H - E_Q$ diagram shows that spin-memory region is restricted by H^{**}

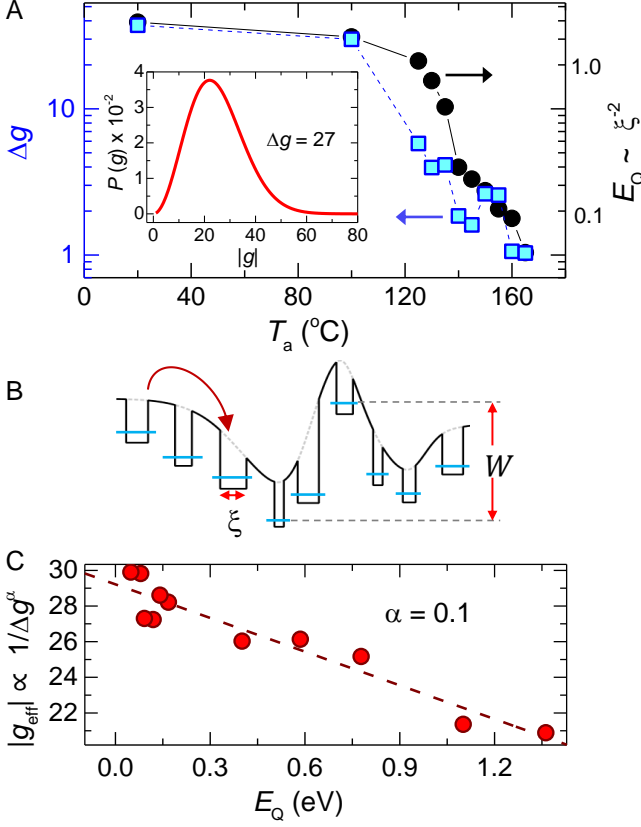


FIG. 3. Distribution of spin g -factors and confinement energy. (A), Width Δg of the g -factor distribution $P(g)$ vs. T_a follows the confinement energy $E_Q(T_a)$. E_Q is modeled by a particle-in-a-box and calculated using ξ as a box size. In the amorphous state in the conduction tail states effective mass is strongly enhanced [28]. Inset: $P(g)$ calculated in the strong SOC regime [29] for $\Delta g = 27$. (B), A model of disorder landscape within the Anderson bandwidth W riding on a long-range smooth potential [30]. (C), Effective g -factor, $|g_{eff}|$, increases with E_Q . We note that the sign of g for many semiconductors, particularly with strong SOC, is negative [4].

to relatively low fields, but when the system is less localized the ‘envelope’ of the spin-memory space switches to H_{max} .

The temperature range over which spin memory is evident is set by the VRH process (Fig. 2B), with $\Delta G_{xx}(H)$ well described by Eq. (1). Above ~ 10 K, outside the VRH region, $\Delta G_{xx}(H)$ becomes nearly ‘flat’ (Fig. 4D); there both τ_s (Fig. S7A) and $|g_{eff}|$ (see Fig. S7B) appear to saturate, and spin-memory phenomenon is not expected. The typical field scale associated with the E-S energy $T_0 \sim 10 - 30$ K is in the 1-2 T range, in close correspondence with H^{**} at low T . As before, $H_{max} \neq H^{**}$, and in the low-temperature localized state H_{max} becomes the limiting crossover field (Fig. 4E). Above $T_a \simeq 180^\circ\text{C}$ ($E_Q \approx 60$ meV), in the strongly disordered *crystalline* state spin memory phenomenon is not detectable. The exit from the spin-memory state

at $\simeq 180^\circ\text{C}$ is clearly evidenced by a transition from the negative MR (neg-MR) to a positive MR (pos-MR) ‘cusp’ characteristic of the WAL state (Fig. 5A). The WAL cusp scales with the transverse component of applied magnetic field $H_\perp = H \cos \theta$ (Fig. 5B), consistent with the 2D (orbital) character expected in a topological insulator [9] under weak disorder. This 2D scaling should be contrasted with isotropic (3D) scaling of the neg-MR peak in the spin-memory state. Thus, unlike the WL-WAL transition driven by magnetic impurities [25], the transition from spin-memory onto a WAL state is also a 3D-2D dimensionality transition at which the electron system rapidly delocalizes. The change of the localization length ξ with decreasing disorder is smooth at the transition to WAL (Fig. 5C), with electron mean free path only limited by the film thickness and grain size in the crystalline state at high T_a (Fig. S8). We remark again that WAL onsets at $\simeq 180^\circ\text{C}$, way above the crystallization transition at $\simeq 140^\circ\text{C}$ (see inset in Fig. 5C), pointing to a disorder threshold for the topological state.

To summarize, we directly detect spin response of the topological material Sb_2Te_3 under strong structural disorder, which we can control and tune by thermal annealing from amorphous to crystalline state. Under strong disorder, the system develops spin-correlations that drive the spin-memory phenomenon controlling the transport of charge. Both in magnetic field and in disorder strength, the parameter space where spin memory exists is unexpectedly broad — it persists well into a disordered crystalline state where, eventually, a 2D WAL quantum interference correction is recovered. While a simple phenomenology we used captures the key features of transport under strong disorder, this regime is undoubtedly complex and theory has yet to provide a full understanding of charge transport under such conditions, particularly when spin-orbit coupling is strong. A new perspective revealed by our findings is that spin-memory effect sets a disorder threshold at which topological protection of the gapless surface states is reclaimed. Save for the edge currents, the control of spin-dependent transport arising from nonequilibrium correlations can, in principle, be achieved by using electrostatic gating [34], and by modifying correlations with an addition of localized spins using currently practiced semiconductor doping techniques.

We wish to acknowledge Roland Winkler for his key insights regarding g -factors. We thank Igor Aleiner and Boris Spivak for their useful comments. We are grateful to Andy Kellock for the RBS and PIXE analysis of the films. This work was supported by the NSF grants DMR-1312483-MWN, DMR-1420634, and HRD-1547830 (L.K.-E.).

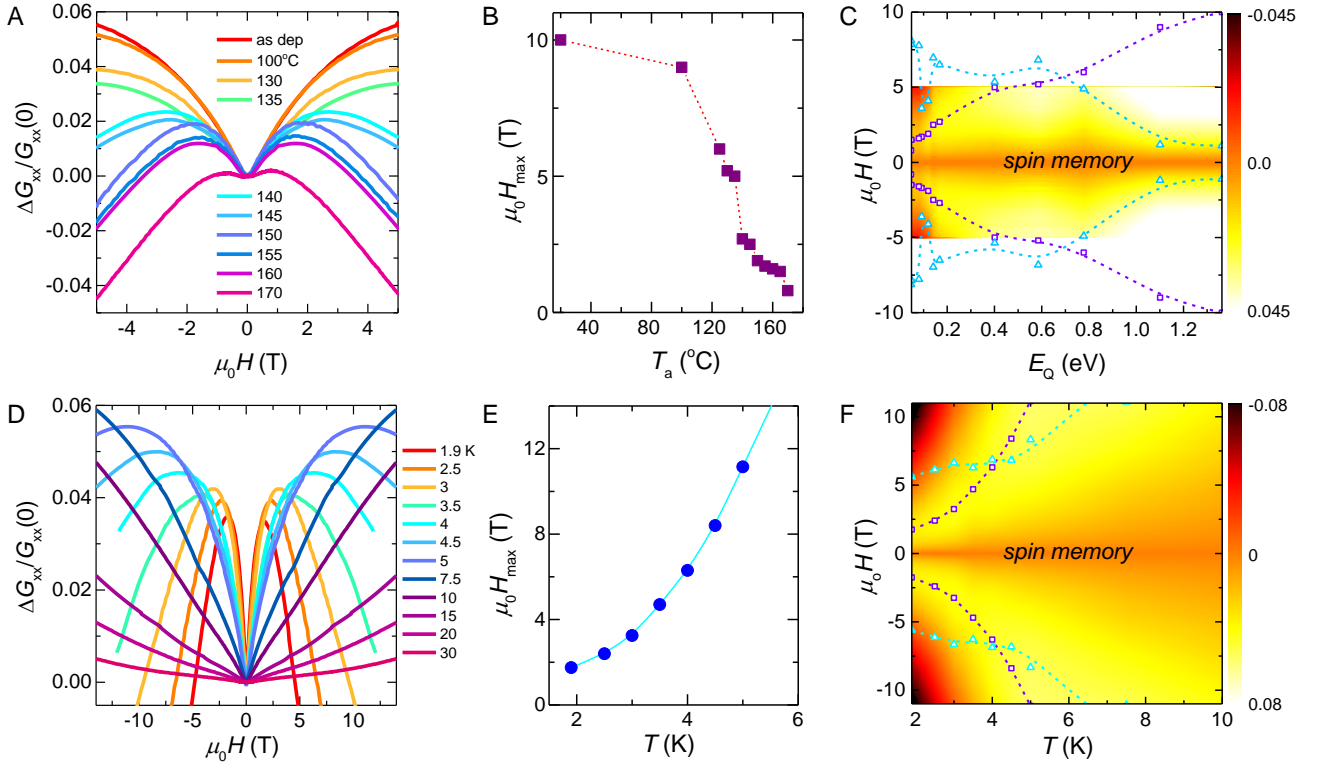


FIG. 4. Phase diagrams of the spin-memory state. (A), Normalized change in $\Delta G_{xx}(H)/G_{xx}(0)$ at 1.9 K for different levels of disorder labeled by T_a . At low disorder the non-analytic positive spin-memory ‘cusp’ transforms into a parabolic form when the huge conductance rise near crystallization is nearly complete. (B), The transformation occurs via reduction of the crossover field H_{max} . (C), Phase diagram in the $H - E_Q$ space showing the huge disorder range where spin memory effect is present. (D), $\Delta G_{xx}(H)/G_{xx}(0)$ shown for $T_a = 150^\circ\text{C}$ at different bath temperatures T . As T increases the spin-memory ‘cusp’ grows and widens until the system exits the VRH regime and enters the regime where transport eventually becomes diffusive. (E), In the VRH range the crossover field H_{max} monotonically increases with T . (F), Phase diagram in the $H - T$ space controlled by spin memory. At low T this range is bounded by $H_{max} \lesssim H^{**}$. The color scales of the contour plots indicate the level of $\Delta G_{xx}(H)/G_{xx}(0)$. H_{max} (hollow purple squares) and the hopping field scale H^{**} (hollow blue triangles) combine to define a limiting envelope for the spin-memory space.

APPENDIX

Film growth and structural characterization. Films of Sb_2Te_3 with thicknesses ranging from 20 to 100 nm were sputter-deposited at room temperature in Ar gas at 4 mTorr and a flow of 46 sccm from a nominally stoichiometric target using 15 W DC power on Si_3N_4 (100 nm)/Si substrates. The stoichiometry was confirmed by Rutherford Backscattering (RBS) and particle induced X-ray emission (PIXE). RBS data were collected at NEC 3UH Pelletron using a Si surface barrier detector with He^+ ions at 2.3 MeV. PIXE data was collected using a Si-Li detector with H^+ ions at 1 MeV. Elemental analysis was done at Evans Analytical Group. X-ray diffraction characterization was performed using Bruker D8 Discover system with the da Vinci configuration using a monochromated beam ($\lambda_{Cu} = 1.5418\text{\AA}$) and a scintillator detector with analyzer crystal (HR-XRD). The film morphology was characterized using the FEI Titan Themis 200 transmission electron microscope (TEM), 200 kV, with TEM

resolution 0.9\AA and $4k \times 4k$ Ceta 16M CMOS camera. Disorder was characterized by Raman spectra using 633 nm linearly polarized excitation in a backscattering configuration [35], with power kept below 2 mW to avoid heating effects.

Magnetic measurements were performed using custom-designed on-chip μ -Hall sensors based on $\text{In}_{0.15}\text{Ga}_{0.85}\text{As}$ heterostructures (SI). To measure magnetization, ~ 50 micron in lateral size thin Sb_2Te_3 film samples were exfoliated from their substrates and placed directly on the SiO_2 -passivated sensor using PDMS. At each temperature an empty twin sensor was used for background subtraction. Transport measurements were performed in a 14 Tesla Quantum Design PPMS system in 1 mTorr of He gas on many film samples, each subjected to the same annealing protocol used to tune the level of disorder. Lithographically patterned structures combining both Hall bar and van der Pauw electrical contact configurations with Ti/Au metallurgy were used (Fig. 2A). Measurements were performed on as-deposited films and on the same

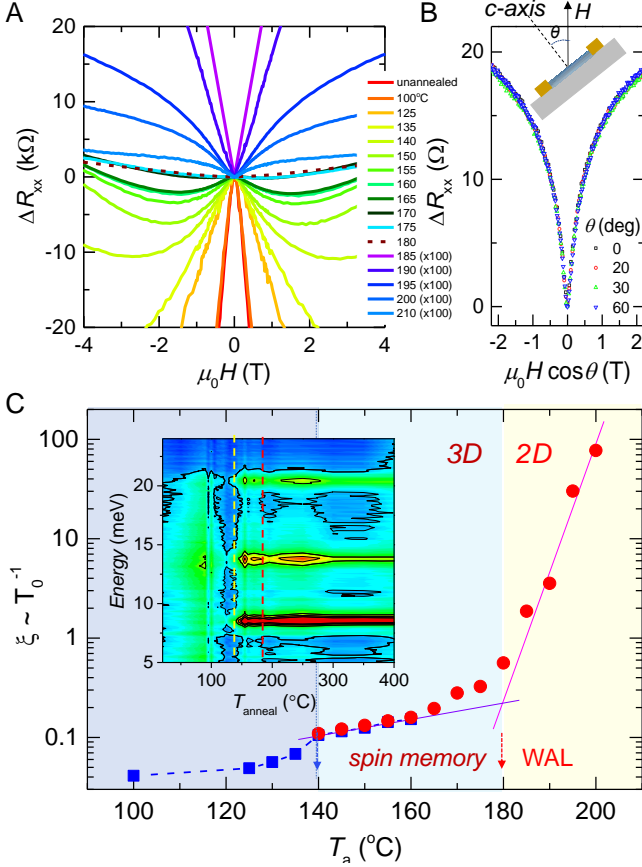


FIG. 5. Transition from the spin-memory to weak antilocalization (WAL) state in disordered crystalline Sb_2Te_3 films. (A), Upon annealing, ΔR_{xx} undergoes transition from the spin memory neg-MR state to a positive magnetoresistance (pos-MR) WAL regime at $T_a \cong 180^\circ\text{C}$, when charge transport becomes diffusive. (B), The WAL pos-MR has a 2D character as evidenced by the scaling with the transverse component of magnetic field. (C), Localization length $\xi \propto T_0^{-1}$ shows a distinct kink at crystallization and a smooth transition to a 2D WAL state. T_0 was obtained from fitting to the E-S VRH formula [30]. Inset: Crystallization at $T_a \cong 140^\circ\text{C}$ (yellow dash) is clearly seen as sharp lines in the Raman spectra *vs.* T_a . Transition to WAL at $\cong 180^\circ\text{C}$ is indicated by red dash.

films after each 5 min annealing step in a box furnace in flowing nitrogen in the temperature range across crystallization at $T_a \sim 140^\circ\text{C}$. We used a numerical Monte Carlo technique to fit our transport data to Eq. (1).

- [1] E. Abrahams, P. Anderson, D. Licciardello, and T. Ramakrishnan, Scaling theory of localization: Absence of quantum diffusion in two dimensions., *Phys. Rev. Lett.* **42**, 673 (1979).
- [2] F. Evers and A. Mirlin, Anderson transitions., *Rev. Mod. Phys.* **80**, 1355 (2008).
- [3] N. Mott, in *Metal-insulator transitions* (Taylor & Francis, New York, 1997).

- [4] R. Winkler, in *Spin-orbit coupling effects in two-dimensional electron and hole systems* (Springer-Verlag, Berlin-Heidelberg-New York, 2003).
- [5] I. Žutić, J. Fabian, and S. Das Sarma, Spintronics: Fundamentals and applications., *Rev. Mod. Phys.* **76**, 323 (2004).
- [6] X.-L. Qi and S.-C. Zhang, Topological insulators and superconductors, *Rev. Mod. Phys.* **83**, 1057 (2011).
- [7] D. Scanlon, P. King, R. Singh, A. de la Torre, S. McKeown Walker, G. Balakrishnan, F. Baumberger, and C. Catlow, Controlling bulk conductivity in topological insulators: key role of anti-site defects., *Adv. Mater.* **24**, 2154 (2012).
- [8] H. Beidenkopf, P. Roushan, J. Seo, L. Gorman, I. Drozdov, Y. S. Hor, R. Cava, and A. Yazdani, Spatial fluctuations of helical Dirac fermions on the surface of topological insulators, *Nature Phys.* **7**, 939 (2011).
- [9] L. Zhao, M. Konczykowski, H. Deng, I. Korzhovska, M. Begliarbekov, Z. Chen, E. Papalazarou, M. Marsi, L. Perfetti, A. Hruban, A. Wołos, and L. Krusin-Elbaum, Stable topological insulators achieved using high energy electron beams., *Nature Comm.* **7**, 10957 (2016).
- [10] I. Lee, C. Kim, J. Lee, S. Billinge, R. Zhong, J. Schneeloch, T. Liu, T. Valla, J. Tranquada, G. Gu, and J. Davis, Imaging Dirac-mass disorder from magnetic dopant atoms in the ferromagnetic topological insulator $\text{Cr}_x(\text{Bi}_{0.1}\text{Sb}_{0.9})_{2-x}\text{Te}_3$, *Proc. Natl. Acad. Sci. (USA)* **112**, 13161321 (2015).
- [11] O. Breunig, Z. Wang, A. Taskin, J. Lux, A. Rosch, and Y. Ando, Gigantic negative magnetoresistance in the bulk of a disordered topological insulator., *Nature Comm.* **8**, 15545 (2017).
- [12] G. Bergmann, Weak localization in thin films: A time-of-flight experiment with conduction electrons., *Phys. Rep.* **107**, 158 (1984).
- [13] L. Zhang, M. Dolev, Q. Yang, R. Hammond, B. Zhou, A. Palevski, Y. Chen, and A. Kapitulnik, Weak localization effects as evidence for bulk quantization in Bi_2Se_3 thin films., *Phys. Rev. B* **88**, 121103(R) (2013).
- [14] J. Li, R.-L. Chu, J. Jain, and S.-Q. Shen, Topological Anderson insulator., *Phys. Rev. Lett.* **102**, 136806 (2009).
- [15] C. Groth, M. Wimmer, A. Akhmerov, J. Tworzydło, and C. Beenakker, Theory of the topological Anderson insulator., *Phys. Rev. Lett.* **103**, 196805 (2009).
- [16] H.-M. Guo, G. Rosenberg, G. Refael, and M. Franz, Topological Anderson insulator in three dimensions., *Phys. Rev. Lett.* **105**, 216601 (2010).
- [17] G. Schubert, H. Fehske, L. Fritz, and M. Vojta, Fate of topological-insulator surface states under strong disorder., *Phys. Rev. B* **85**, 201105(R) (2010).
- [18] N. P. Mitchell, L. M. Nash, D. Hexner, A. M. Turner, and W. T. M. Irvine, Amorphous topological insulators constructed from random point sets., *Nature Phys.* **14**, 1 (2018).
- [19] A. Agarwala and V. B. Shenoy, Topological insulators in amorphous systems., *Phys. Rev. Lett.* **118**, 236402 (2017).
- [20] H. Zhang, C. Liu, X.-L. Qi, X. Dai, Z. Fang, and S.-C. Zhang, Topological insulators in Bi_2Se_3 , Bi_2Te_3 , and Sb_2Te_3 with a single Dirac cone on the surface., *Nature Phys.* **5**, 438 (2009).
- [21] D. Hsieh, Y. Xia, D. Qian, L. Wray, F. Meier, J. Dil, J. Osterwalder, L. Patthey, A. Fedorov, H. Lin, A. Bansil, D. Grauer, Y. Hor, R. Cava, and M. Hasan, Observation

- of time-reversal protected single-Dirac-cone topological-insulator states in Bi_2Te_3 and Sb_2Te_3 , *Phys. Rev. Lett.* **103**, 146401 (2009).
- [22] L. Zhao, H. Deng, I. Korshovska, Z. Chen, M. Konczykowski, A. Hruban, V. Oganessian, and L. Krusin-Elbaum, Singular robust room-temperature spin response from topological Dirac fermions., *Nature Mater.* **13**, 580 (2014).
- [23] O. Agam, I. Aleiner, and B. Spivak, Spin-memory effect and negative magnetoresistance in hopping conductivity., *Phys. Rev. B* **89**, 100201(R) (2014).
- [24] B. Shklovskii and A. Efros, in *Electronic properties of doped semiconductors* (Springer-Verlag, Berlin, 1984).
- [25] M. Liu, J. Zhang, C.-Z. Chang, Z. Zhang, X. Feng, K. Li, K. He, L.-L. Wang, X. Chen, X. Dai, Z. Fang, Q.-K. Xue, X. Ma, and Y. Wang, Crossover between weak antilocalization and weak localization in a magnetically doped topological insulator., *Phys. Rev. Lett.* **108**, 036805 (2012).
- [26] Z. Chen, S. Carter, R. Bratschitsch, P. Dawson, and S. Cundiff, Effects of disorder on electron spin dynamics in a semiconductor quantum well., *Nature Phys.* **3**, 265 (2007).
- [27] D. Shakhvorostov, R. Nistor, L. Krusin-Elbaum, G. Martyna, D. Newns, B. Elmegreen, X.-H. Liu, Z. Hughes, S. Paul, C. Cabral, S. Raoux, D. Shrekenhamer, D. Basov, Y. Song, and M. Müser, Evidence for electronic gap-driven metal-semiconductor transition in phase-change materials., *Proc. Natl. Acad. Sci. (USA)* **106**, 10907 (2009).
- [28] J. Singh, Effective mass of charge carriers in amorphous semiconductors and its applications., *J. Non-Cryst. Solids* **299-302**, 444 (2002).
- [29] S. Csonka, L. Hofstetter, F. Freitag, S. Oberholzer, C. Schönenberger, T. Jespersen, M. Aagesen, and J. Nygård, Giant fluctuations and gate control of the g-factor in InAs nanowire quantum dots., *Nano Lett.* **8**, 3932 (2008).
- [30] V. Gantmakher, in *Electrons and disorder in solids* (Clarendon Press, Oxford, 2005).
- [31] L. Ioffe and B. Spivak, Giant magnetoresistance in the variable-range hopping regime., *J. Exp. Theor. Phys.* **117**, 551 (2013).
- [32] S. Havlin and D. Ben-Avraham, Diffusion in disordered media., *Adv. Phys.* **51**, 187 (2002).
- [33] A. Woloś, S. Szyszko, A. Drabinska, M. Kaminska, S. Strzelecka, A. Hruban, A. Materna, M. Piersa, J. J. Borysiuk, K. Sobczak, and M. Konczykowski, g-factors of conduction electrons and holes in Bi_2Se_3 three-dimensional topological insulator., *Phys. Rev. B* **93**, 155114 (2016).
- [34] J. Sandhu, A. Heberle, J. Baumberg, and J. Cleaver, Gateable suppression of spin relaxation in semiconductors., *Phys. Rev. Lett.* **86**, 2150 (2001).
- [35] J. Secor, M. Harris, L. Zhao, H. Deng, S. Raoux, and L. Krusin-Elbaum, Phonon renormalization and Raman spectral evolution through amorphous to crystalline transitions in Sb_2Te_3 thin films., *Appl. Phys. Lett.* **104**, 221908 (2014).